Numerical Study of Half Wavy and Half W-type Collecting Plates on the Characteristics of Electrostatic Precipitators

Angel Asipuela[1*], Tamás Iváncsy[1]

[1] Department of Electric Power Engineering, Faculty of Electrical Engineering and Informatics, Budapest University of Technology and Economics, Műegyetem rkp. 3., H-1111 Budapest, Hungary
* Corresponding author, e-mail: gabriel.bme_2020@edu.bme.hu

Abstract

Many industries rely heavily on ESPs (electrostatic precipitators). They exist primarily as air filters to prevent hazardous particles from entering the environment. Duct-type ESPs are widely used, have a simple design, and rely on corona wires and collecting plates as their primary arrangement. Numerous studies have been conducted to demonstrate that changing the geometrical shape can aid in improving particle collection efficiency. Wavy plates, W-types, and other designs, for example, have shown to improve particle collection efficiency in a positive degree. The goal of this study is to see what happens when two different types of collecting plates are combined and used together. The proposal is to combine half wavy and half W-type collecting plates and examine them with corona wires with circular shapes. As a result, after completing the numerical study and comparing the results, it is clear that the levels of particle collection efficiency for the various particle sizes have increased with this proposed design. Furthermore, six cases are presented with this design, and the results describe the electrical properties and their magnitude distributions. In fact, in all of the cases presented, this type of combination increased particle collection efficiency.

Keywords

ESP, corona discharge, collecting electrodes, particle collection

1 Introduction

The importance of ESP stems from its ability to collect air pollutants from industries, reducing pollution released into the environment. This equipment is characterized by its high efficiency. However, ESP efficiency is reduced because micro-particles with a radius of about 0.2 um are difficult to capture due to their nature; however, various studies are being conducted to increase particle collection efficiency.

Since ESPs have been used in the industry for many years, a description of how they work will be described. For instance, White [1] explains the fundamentals of ESP operation, as well as its foundational mathematical models and operational conditions in his book. New models for particle charging, particle collection, and fluid flow have been proposed in current investigations to improve the approximation with experimental results. However, the fundamental concepts are still present. For example, boundary conditions, the usage of negative corona discharge for a better performance [2], and also Peek's law, which describes the onset electric field [1–7]. Certain studies show how changes in the geometric design of

ESPs affect their electrical properties while also helping to boost their efficiency levels, then the question of how to improve ESP performance with a better design is brought. According to the research of Gao et al. [8], changing electrode configurations can affect particle migration. This study used corona electrodes of circular, square, 45° square, and needle forms. In case of collecting plates, they used FP (flat plates) and sigma type collecting plates. The results show that changing the geometry of collecting plates and/or corona wires can modify the characteristics of ESPs. The study emphasizes, particle migration and particle collection efficiency where higher levels are found on needle wires with sigma type collecting plates [8].

Corona wires with pointed and flat ends were arranged in symmetric and asymmetric double columns. Tong et al. [9] changed the shape of the corona wires and tested them in honeycomb tube ESP. Four study cases were done in total. In conclusion, it is stated how an asymmetric configuration with corona wires with pointed ends enhances an optimized design. Also, collection efficiency increases

linearly from 10 kV to 50 kV. In addition, the study describes that uniformity of the electric field decreases as the incoming gas velocity increases from 0.5 to 1 m/s [9]. Based on Wang et al. [10], ESP can be improved by encouraging particle matter growth and agglomeration (CPM). This could be achieved by lowering the temperature and increasing the humidity. Prechargers are another option for dealing with ultra-fine particles. Furthermore, it was recommended for ESP designs that small distances between corona wires and collecting plates be considered to improve particle collection, and spike and arista electrodes are a feasible alternative to corona wires [10]. Choi et al. [11] demonstrated in a numerical simulation using wavy collecting plates that while volumetric flow reduces particle collection efficiency, applied voltage increases particle collection efficiency. The wavy shape improves particle charging and collection. This analysis determined that the case Wavy-E had the best effect, so this model was used to define the geometry for the wavy and W-type shapes in this current and previous papers [11]. Zhou et al. [12], for example, assessed the performance of FPs, C-type, triangular type, W-type, corrugated type, and crenelated type. They concluded that the shape of the collecting plates has a significant influence on the intensity of the electric field. The distribution of the electric field in flat, C-type, and W-type collecting plates makes the electric field more uniform. The ESP with triangular collecting electrodes provides the highest particle collection efficiency for dust particles of different sizes [12].

A laminar flow concept can be used to define the fluid flow in an ideal situation, but °it will not accurately represent the operation of an ESP in real conditions. As a result, turbulent flow is used to simulate many numerical study cases. Additionally, the transport equation that describes the distribution of the electric potential and space charge density is defined by the fluid's velocity [5, 13]. According to Wang [14], who discussed the impacts of altering the corona distribution, the efficiency of the collection is increased by increasing the number of corona electrodes in relation to the length and spacing between the collecting electrodes. Taking as reference Wang's results [14], the cases 'a' to 'f' are the references for this study. It has been demonstrated that changes in the geometry of the ESP lead to increase particle collection levels. For instance, triangular plates (TPs), demonstrated that minimal changes to the geometry increase particle collecting efficiency as compared to wavy and W-type plates where the geometries of these plates are considerably altered [15]. Therefore, the proposal

is to combine different designs, as in the case of W-type and wavy collecting plates and analyze how this combination increases or decreases particle collection. These two models improve particle collection efficiency based on previous studies [14]. Combining these ideas with our prior research on W-type and wavy collection plates [16]. There are a few different combinations that could work, however for this study the length of the collecting plates will be made with half wavy and the other half with a W-type shape; this sequence was chosen without preference. The objective is to assess what occurs if more geometries are combined. The results obtained by numerical study focus on analyzing the distribution of electric characteristics including electric potential, space charge density, electric field, current density, and particle collection efficiency.

2 Numerical methodology
2.1 Corona discharge
Each stage or component of an ESP is represented by a different mathematical model. For instance, Poisson's equation and the charge conservation equation are used to model the corona discharge, which is an electrical phenomenon that happens at a stage not too far from a complete discharge or spark. These equations do, however, mainly represent the electrical properties when a corona discharge occurs. Eqs. (1) and (2) are the Poisson and charge conservation equations respectively, besides, Eqs. (3) and (4) are associated with Eq. (1):

$$\frac{\partial \rho_q}{\partial t} + \nabla \times \boldsymbol{J} = 0, \tag{1}$$

$$\boldsymbol{J} = z_q \mu \rho_q \boldsymbol{E} + \rho \boldsymbol{u}, \tag{2}$$

$$\varepsilon_0 \nabla^2 V = -\rho_q, \tag{3}$$

$$\boldsymbol{E} = -\nabla V, \tag{4}$$

where ρ_q(C m³) is the space charge density, $\boldsymbol{J}$(A m⁻²) is the current density, z_q is the charge number, μ(m² V⁻¹ s⁻¹) is the ion mobility, $\boldsymbol{E}$(V m⁻¹) is the electric field, $\boldsymbol{u}$(m s⁻¹) is the fluid velocity, ε_0(F m⁻¹) is the free-space permittivity, and V(V) is the electric potential [17].

Boundary conditions must be established in order to solve these equations; the first boundary condition is defined by using Peek's equation (Eq. (5)), which states that the onset electric field relies on the corona wire's radius and the environment conditions in which it operates. In this case, ($\boldsymbol{n} \times \boldsymbol{E} = E_0$), and E_0 is directly calculated by Eq. (5):

$$E_0 = 3 \times 10^6 \delta \left(1 + \frac{0.03}{\sqrt{\delta \times r_w}} \right), \tag{5}$$

$$\delta = \frac{T_0}{T} \times \frac{P}{P_0}, \tag{6}$$

where $E_0 (\text{V m}^{-1})$ is the constant electric field on the corona electrode, n is a normal unit vector, $r_w (\text{m})$ is the corona wire radius, δ is a relation between $T_0 (293.15 \text{ K})$ the absolute temperature and $P_0 (760 \text{ mmHg})$ the normal atmospheric pressure, with P and T which are the operating values. The other boundary conditions are determined by the voltage applied to the corona wires and the grounded collecting plates $V: V = V_0$ and $V = 0 (\text{V})$ [18, 19]. Additionally, the inlet and outlet of the model are defined as having zero charges.

Fig. 1 depicts the space charge distribution for cases 'a' to 'f' as we continue with this investigation. The results obtained with this proposed design can be seen in comparison to the results from FPs.

2.2 Fluid flow
Laminar flows are desirable, thus a turbulent flow is preferable for this investigation. Then, an incompressible, stable, and turbulent flow is defined using the RNG method and the *k-epsilon* turbulence model.

$$\rho \nabla \times \boldsymbol{u} = 0, \tag{7}$$

$$\rho \frac{\partial \boldsymbol{u}}{\partial t} + \rho (\boldsymbol{u} \times \nabla) \boldsymbol{u}$$
$$= \nabla \times \left[-p\boldsymbol{I} + \mu_f \left(\nabla \boldsymbol{u} + (\nabla \boldsymbol{u})^T \right) \right] + \boldsymbol{F}_{EHD}, \tag{8}$$
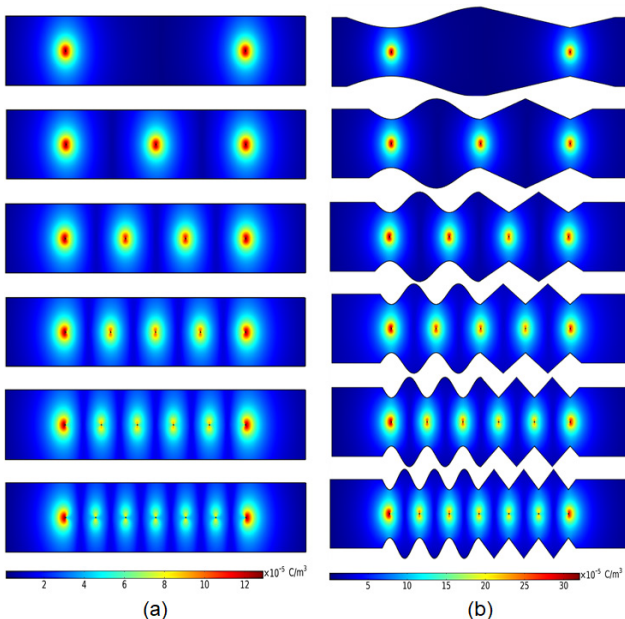
Fig. 1 Space charge distribution using (a) FPs and (b) wavy-W-typePs

$$\boldsymbol{F}_{EHD} = \rho_q \boldsymbol{E}, \tag{9}$$

where $\rho (\text{kg m}^{-3})$ is the fluid density, $p (\text{Pa})$ is the pressure, $\mu_f (\text{kg m}^{-1} \text{ s}^{-1})$ is the dynamic viscosity, $\boldsymbol{I}$ is the identity matrix, and $\boldsymbol{F}_{EHD}$ is the electrohydrodynamic force [17].

2.3 Particle charging
Another important topic is particle charging, which occurs when particles begin to collect charges as they cross and enter the ionized field and could be thoroughly explained by several mathematical equations. These models can estimate the charging rate and the amount of charges that the particles can have. There are two types of particle charging mechanisms that take effect. These particles can be charged using a thermal process called diffusion charging and/or a field charging process. Ions colliding with dust particles and charging them, and also thermal movement charges them by transferring their charge to them [1]. The Lawless model considers large and small particles, is a preferred representation for estimating the field and diffusion charging process on particles [10, 17, 19, 20], in this paper Lawless' model is used to estimate particle charging process:

$$\tau_c \frac{dZ}{dt} = \begin{cases} \dfrac{v_s}{4\varepsilon_0} \left(1 - \dfrac{v_e}{v_s} \right)^2 + f_a, & \left(|v_e| \le |v_s| \right) \\[3mm] \dfrac{v_e - v_s}{\exp(v_e - v_s) - 1} f_a, & \left(|v_e| > |v_s| \right) \end{cases}, \tag{10}$$

$$\tau_c = \frac{e^2}{4\pi \rho_q \mu k_B T_i}, \tag{11}$$

where τ_c is the charging time, Z is the charge number, k_B is the Boltzmann's constant, and T_i is the ion temperature:

$$v_s = 3w_e \frac{\varepsilon_{r,p}}{\varepsilon_{r,p+2}}, \tag{12}$$

$$v_e = \frac{Ze^2}{4\pi \varepsilon_0 r_p k_B T_i}, \tag{13}$$

$$w_e = \frac{er_p |E|}{k_B T_i}, \tag{14}$$

where v_e is the self-potential of the particle, w_e is the dimensionless electric field intensity, $\varepsilon_{r,p}$ is the relative permittivity of the particles, f_a is an analytic fitting function which is depending on w_e and e is the elementary charge [17, 21].

$$f_a\left(w_e\right) \equiv \begin{cases} \dfrac{1}{\left(w_e + 0.475\right)^{0.575}}, & w_e \geq 0.525 \\ 1, & w_e < 0.525 \end{cases}, \qquad (15)$$

2.4 Particle kinetics

Each charged particle will be mainly affected by the electric force and the mechanical force resulting from the fluid flow, besides, gravity is not taken into account when particles pass through the ESP. These two types of forces are defined in Eqs. (18) and (20). When electrical forces interact, charged particles will tend to move as quickly as possible toward the collecting plates due to the attraction forces of opposite charges. Initially, the particles would try to follow the direction of the gas flow until they were charged. Newton's second law, which can be found in Eq. (16), describes particle motion:

$$\frac{d\boldsymbol{x}}{dt} = \boldsymbol{v}, \qquad (16)$$

$$\frac{d}{dt}\left(m_p \boldsymbol{v}\right) = \boldsymbol{F}_t, \qquad (17)$$

where $\boldsymbol{x}$(m) is the particle position, $\boldsymbol{v}$(m s^{-1}) is the particle velocity, m_p(kg) is the mass of the particle, and $\boldsymbol{F}_t$(N) is the total force on the particle.

The drag force $\boldsymbol{F}_D$(N) is defined by Eq. (18), which includes corrections defined by the Cunningham-Millikan-Davis model [17], and the electric force $\boldsymbol{F}_e$(N) is described by Eq. (20):

$$\boldsymbol{F}_D = \frac{1}{\tau_p S} m_p \left(\boldsymbol{u} - \boldsymbol{v}\right), \qquad (18)$$

$$\tau_p = \frac{4\rho_p d_p^2}{3\mu C_D Re_r}, \qquad (19)$$

$$\boldsymbol{F}_e = eZ\boldsymbol{E}, \qquad (20)$$

where τ_p(s) is the particle velocity-time response; S is the drag correction coefficient, ρ_p(kg m^{-3}) is the density of the particles; d_p(m) is the particle diameter; C_D is the Cunningham correction factor; and Re_r is the Reynolds number, e(C) is an elementary charge and Z is the accumulated charge number on the particle [12, 17, 22].

2.5 Particle collection

The performance of the ESP is, in fact, assessed by how many particles have been captured and how many have not. Probability theory can be used to evaluate this.

For instance, Eq. (21) can be used to calculate particle collection efficiency for a duct-type ESP, this equation is dependent on the length, the distance between one corona wire and one of the collecting plates, and also the velocities of the particles and gas, respectively [23, 24]. However, due to the geometrical modifications for this study, this equation may not give a good approximation, using software, particle collection efficiency is determined by counting the particles at the ESP's outlet:

$$\eta = 1 - \exp\left(-\frac{L \times |\boldsymbol{v}|}{s \times |\boldsymbol{u}|}\right). \qquad (21)$$

2.6 Geometry and parameters definition

All of the preceding stages occur in order, but they are also interdependent. How can all of this be brought together? Fortunately, we have access to software tools that make it simple to solve these models, for example, the results of some models are used as input for the models that follow, implying that the study can be carried out individually. Furthermore, each model is performed on each case study shown in Fig. 2.

2.7 The applied and sparkover voltages

The applied voltage has been kept as a constant value to evaluate the effects of this combination on the electric properties. However, the position of the corona wires could be shifted to the right or left to avoid being close to the spark voltage region. The particle collection efficiency is directly related to the voltage as shown in some studies [11, 24]. In case of moving the corona electrodes if the voltage is kept constant the particle collection efficiency will be decreased. In this case, the applied voltage must be increased, however, the sparkover region must be defined based on the shortest distances between the corona electrodes and collecting plates. However, for what is described experimentation will be needed. Fig. 3 shows three possible positions for the corona electrodes and the shortest distances to be considered for an applied voltage.

In this study, a two-dimensional model is used to evaluate a combination model that uses half wavy and half W-type. Six cases are studied, denoted by the letters 'a' to 'f' (see Fig. 2). Each case is differentiated by the number of corona electrodes specified by the L_{ww}/L_{wp} relationship (L_{ww}: distance between two corona wires, L_{wp}: distance between one corona wire and one collecting plate). In this case, a lower L_{ww}/L_{wp} value indicates a higher number of corona wires. The number of corona electrodes for each of the six cases is as follows: case a: 2, case b: 3, case c: 3, case d: 4, case e: 5, and case f: 6. In all cases, the radius
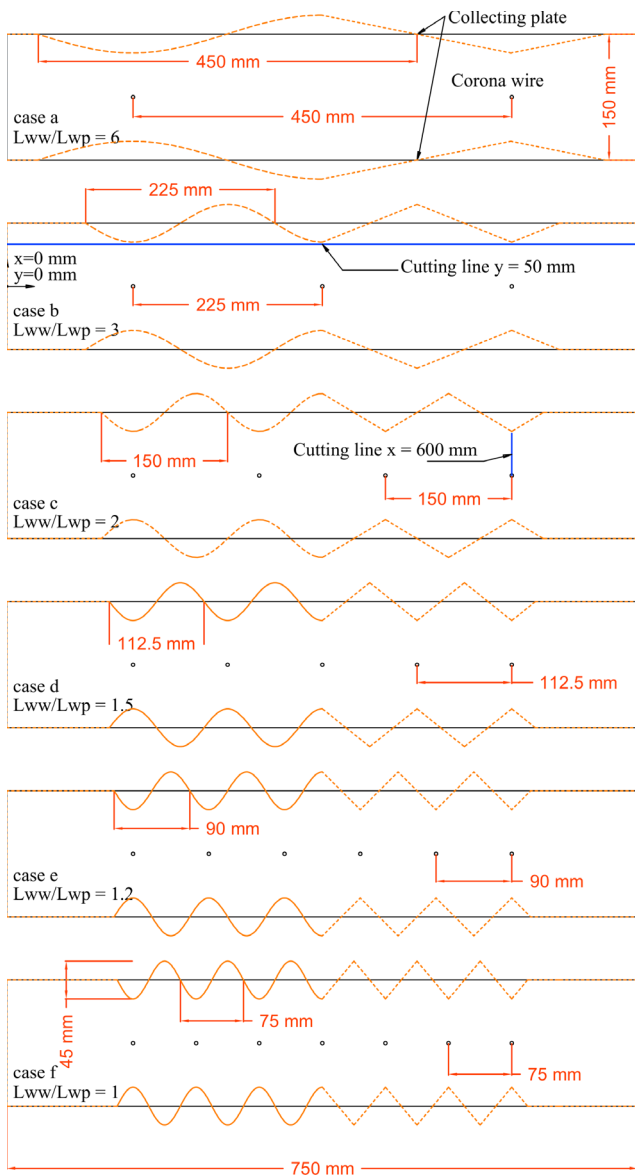
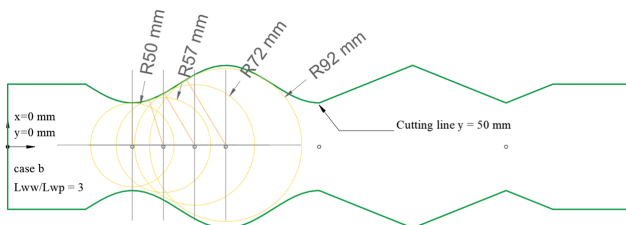**Fig. 2** Geometrical configuration of FPs and wavy-W-typePs

Fig. 3 Displacement of the position of the corona electrodes using wavy-W-types plates

Table 1 Specific geometry for the ESP arrangement

Description	Value
Length (mm)	750
Distance between the collecting plates (mm)	150
Distance between two corona wires (mm)	450; 225; 150; 112.5; 90; 75
Number of corona electrodes	2; 3; 4; 5; 6; 7
Corona electrode radius (mm)	0.75
Applied voltage (kV)	45
Air turbulent fluid flow, avg velocity (m/s)	1
Temperature (K)	293.15
Gas density (kg m^{-3})	1.2
Gas viscosity (Pa s)	1.85×10^{-5}
Pressure (atm)	1
Particle diameter (μm)	0.01^{-5}
Particle density (kg m^{-3})	2200
Particle relative permittivity	5
Reduced ionic mobility (m^{-1} V^{-1} s^{-1})	3×10^{21}
Space charge density, initial value (C m^{-3})	1×10^{-5}

collecting plate is 150 mm, and each plate has a length of 750 mm. The particles have a mass density of 2200 kg/m^3 and a relative permittivity of 5. Typically, it is assumed that the particles have homogeneous radii between 0.01 and 5 um and are spherical in shape. An air turbulent fluid flow is defined for the gas flow with a k-RNG type, 1.2 kg/m^3 gas density, 1 m/s average velocity, and 2.57×10^{-7} Pa s gas viscosity. The operating conditions are 293.15 K temperature and 1 atm pressure.

3 Results and discussion

We proposed comparing the electric potential distribution from a simulation with the experimental data from Penney's research in order to validate our results [25]. The simulation was carried on based on the following parameters: 150 mm distance between two corona wires, 228.6 mm width, 609.6 mm length, and 0.15 mm corona wire radius which are also implemented in Penney's experiment. The numerical result is consistent with the experimental data obtained, see Fig. 4.

3.1 Electric field distribution using wavy-W-typePs

Higher magnitude values are anticipated in wavy-W-typePs due to the shorter distance, which is in line with the concept that the electric field is inversely proportional to the distance between two electric potentials. A horizontal cut is made at y = 50 mm in the wavy-W-typePs design for all cases to obtain the following results, the results for FPs were obtained in previous studies, and it was shown that higher values of
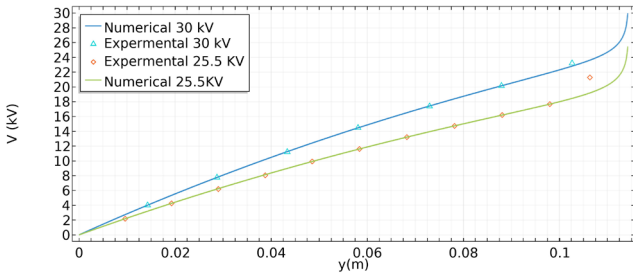
of the corona wires is set to 0.75 mm. The gas flow inlet is set on the left side, and the outlet is set on the right. Furthermore, the plates will be referred to as wavy-W-typePs, a combination of the two. The geometry and operating parameters, such as temperature and pressure, were defined based on previous studies as a guide. it is summarized in Table 1. For instance, the distance between each

Fig. 4 Numerical simulation in comparison with Penney's experimental results, electrical potential distribution between the corona wire and collecting electrode

Fig. 6 Current density distribution using wavy-W-typePs

Fig. 7 Space charge density distribution using wavy-W-typePs

the electric field are obtained using wavyPs or W-typePs. The cases with wavy-W-typePs have much higher magnitude values when it comes to FPs [11, 16]. If we focus on the maximum points of the electric field at x = 150 mm, see Fig. 5, it is found that the lowest electric field value is obtained when $L_{ww}/L_{wp} = 6$, and the highest electric field value is obtained when $L_{ww}/L_{wp} = 1$. Fig. 5 illustrates the distribution of the electric field peaks in relation to the number of corona wires. This design specifies that the first three corona wires correspond to the wavyPs design, while the following three corona wires correspond to the W-typePs design. Let's examine the $L_{ww}/L_{wp} = 1$ case. It can be observed an increase in the magnitude of the highest values of electric field (peaks), the first change happens in the range between x: 300 mm and 400 mm. 1.28×10^6 (V/m) to 1.32×10^6 (V/m), for instance. It can be seen this increase in magnitude for the other L_{ww}/L_{wp} cases as well. In addition, the wavyPs section's electric field distribution is smoother than the W-typePs section's; as an example, consider the $L_{ww}/L_{wp} = 2$ case.

3.2 Current density and space charge density distribution

Figs. 6 and 7, respectively, show how current density and charge space density are distributed. For each of the six cases, higher magnitude current density values are positioned along the corona's wire axis.

Consider the case $L_{ww}/L_{wp} = 1.2$ to see what happens to the electric current density with this combination of wavyPs and W-typePs.
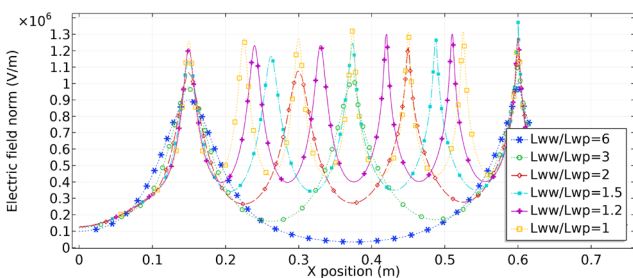

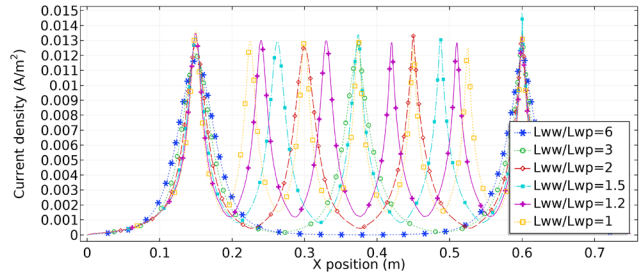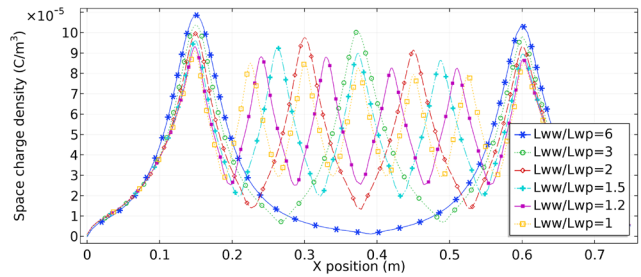**Fig. 5** Electric field distribution using wavy-W-typePs

In the range x: 100 mm and 400 mm it is observed that the magnitudes of electric current in the peaks for the first three crown wires are similar, in the following range x: 400 mm and 700 mm it is found that the following three crowns have similar values also between them, comparing these two ranges, it happens that there is a decrease in the magnitude of the electric current density.

Since in this particular situation $L_{ww}/L_{wp} = 1.2$, the corona wires at the beginning and end present values that are of a magnitude higher than those found inside, it was not possible to generalize the results to the other cases. If the corona wires at the ends are ignored, it is clear that the values of electric current density decrease while changing from a wavyPs design to a W-typePs design. For the cases of $L_{ww}/L_{wp} = 1$ and $L_{ww}/L_{wp} = 1.2$, this criteria is fulfilled. On contrary, the current density increases when the wavyPs are changed out for W-typePs in the cases where $L_{ww}/L_{wp} = 1.5, 2, 3,$ and 6. This transition between wavyPs and W-typePs leads the electric current density to decrease if the distance between the corona electrodes is shorter; on the other hand, it increases if larger distnace are present.

In the case of space charge density, for instance, consider two specific cases (see Fig. 7) $L_{ww/wp} = 1.2$ and 2, and indeed the outer corona wires' space charge densities are significantly higher than those of the inner, which should be excluded for purpose of analyzing. The space charge density maximum values decrease as wavyPs change to W-typePs. Similar situations apply to other L_{ww}/L_{wp} cases. If the corona wires at the ends are not taken into account, it is then clear that there is a decrease in the space charge density for all cases. Additionally, it can be seen that the

minimum values in this space charge density distribution are consistent in every specific case; no significant variation is seen to be described.

3.3 Particle collection efficiency

When taking into account previous studies, the majority of designs or changes made to the collecting plates have a favorable impact on particle collection efficiency. When FPs are used, the particle collection efficiency values are at their lowest. Fig. 8 illustrates the particle collection efficiency of wavy-W-typePs (wWPs) and FPs for all particle sizes studied in this paper along with the cases 'a' to 'f'. All cases show an increase in particle collection efficiency. However, there is a notable increase, especially in the range of 0.5 um particles for all cases.

Fig. 9 represents wavy-W-typePs (wWPs) particle collection efficiency as well as previous studies on FPs, TPs, and W-typePs. The particle size is specified as 0.01 to 0.5 um, but only the cases for 0.05, 0.1, and 0.5 um are shown in Fig. 9. Each case is colored by one similar color, and the dotted bars represent the results using wavy-W-typePs.

4 Conclusions

The proposed design of this combination of half wavy and half W-type collecting plates has a positive impact on the objective of increasing particle collection efficiency levels. Furthermore, the electrical properties of this design are summarized as follows:

- Electric field: without considering the corona wires at the ends, the magnitude values in the wavy plates section are lower than those in the W-typePs section. This happens in all of the cases presented in this study.
- Current density: when $L_{ww}/L_{wp} = 1$ or 1.2, the magnitude values decrease when changing from wavyPs to W-typePs. On the contrary, when $L_{ww}/L_{wp} = 1.5, 2, 3, 6$, the magnitude values increase in the W-typePs section.
- Space charge density: higher magnitude values are found in W-typePs than in the wavyPs section. For this affirmation, the corona wires at the ends should be excluded.
- The wavy-W-typePs model outperforms the other designs in terms of particle collection efficiency. The model can then be highlighted for future research.
- The position of the corona electrodes could be shifted to deal with the sparkover voltage region; however, further investigation is needed to define the relationship between the sparkover and the shortest distances under the conditions of this proposed design.

Finally, as part of our study design group, the design of the combination of two collector plates leads to a positive approach in increasing particle collection efficiency. Further to that, this study was conducted to support future studies and to propose new design combinations.
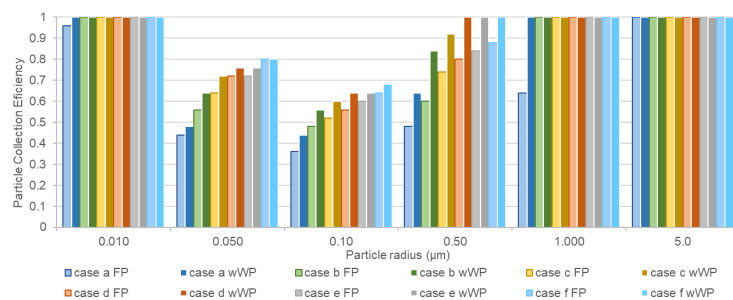
Fig. 8 Particle collection efficiency using wavy-W-typePs compared with FPs
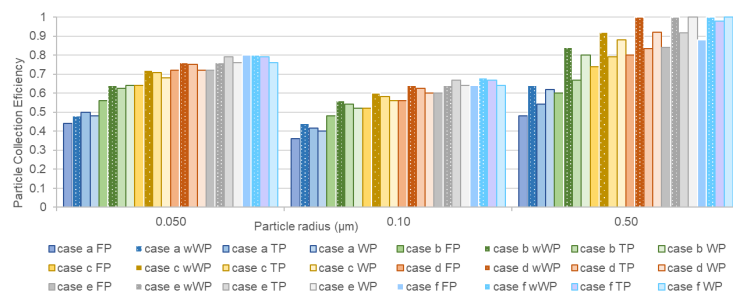

Fig. 9 Particle collection efficiency using wavy-W-typePs compared with FP, WP, and TP

References

[1] White, H. J. "Particle Charging in Electrostatic Precipitation", Transactions of the American Institute of Electrical Engineers, 70(2), pp. 1186–1191, 1951.

[2] Asipuela, A., Iváncsy, T. "Study and Numerical Simulation of Negative and Positive Corona Discharge: A Review", Periodica Polytechnica Electrical Engineering and Computer Science, 66(3), pp. 294–300, 2022.
https://doi.org/10.3311/PPee.19952

[3] White, H. J. "Industrial Electrostatic Precipitation", Addison-Wesley Publishing Company, Reading, MA, USA, 1963.

[4] White, H. J. "Precipitator Design", Journal of the Air Pollution Control Association, 27(3), pp. 206–217, 1977.
https://doi.org/10.1080/00022470.1977.10470412

[5] Feldkamp, M., Dickamp, M., Moser, C. "CFD simulation of electrostatic precipitators and fabric filters state of the art and applications", In: Yan, K. (ed.) Electrostatic Precipitation: 11th International Conference on Electrostatic Precipitation, Hangzhou, 2008, Springer, 2009, pp. 141–150. ISBN 978-3-540-89250-2
https://doi.org/10.1007/978-3-540-89251-9_30

[6] Böttner, C.-U. "The role of the space charge density in particulate processes in the example of the electrostatic precipitator", Powder Technology, 135-136, pp. 285–294, 2003.
https://doi.org/10.1016/j.powtec.2003.08.020

[7] Asipuela, A., Iváncsy, T. "Study and numerical simulation of the electrical properties of a duct-type electrostatic precipitator using seven circular corona wires: A review", Periodica Polytechnica Electrical Engineering and Computer Science, 66(3), pp. 286–293, 2022.
https://doi.org/10.3311/PPee.19482

[8] Gao, W., Wang, Y., Zhang, H., Guo, B., Zheng, C., Guo, J., Gao, X., Yu, A. "Numerical simulation of particle migration in electrostatic precipitator with different electrode configurations", Powder Technology, 361, pp. 238–247, 2020.
https://doi.org/10.1016/j.powtec.2019.08.046

[9] Tong, Y., Liu, L., Zhang, L., Bu, S., Chen, F., Shao, W., Feng, C., Xu, W., Qi, S., Fu, L. "Separation of fine particulates using a honeycomb tube electrostatic precipitator equipped with arista electrodes", Separation and Purification Technology, 236, 116299, 2020.
https://doi.org/10.1016/j.seppur.2019.116299

[10] Wang, Y., Zhang, H., Gao, W., Shao, L., Wu, Z., Zhao, Z., Ge, C., Hu, D., Zheng, C., Gao, X. "Improving the removal of particles via electrostatic precipitator by optimizing the corona wire arrangement", Powder Technology, 388, pp. 201–211, 2021.
https://doi.org/10.1016/j.powtec.2021.04.087

[11] Choi, H. Y., Park, Y. G., Ha, M. Y. "Numerical simulation of the wavy collecting plate effects on the performance of an electrostatic precipitator", Powder Technology, 382, pp. 232–243, 2021.
https://doi.org/10.1016/j.powtec.2020.12.070

[12] Zhou, W., Jiang, R., Sun, Y., Chen, B., Liu, B. "Study on multi-physical field characteristics of electrostatic precipitator with different collecting electrodes", Powder Technology, 381, pp. 412–420, 2021.
https://doi.org/10.1016/j.powtec.2020.12.028

[13] Fujishima, H., Ueda, Y., Tomimatsu, K., Yamamoto, T. "Electrohydrodynamics of spiked electrode electrostatic precipitators", Journal of Electrostatics, 62(4), pp. 291–308, 2004.
https://doi.org/10.1016/j.elstat.2004.05.006

[14] Wang, X. "Effects of corona wire distribution on characteristics of electrostatic precipitator", Powder Technology, 366, pp. 36–42, 2020.
https://doi.org/10.1016/j.powtec.2020.02.044

[15] Fayyad, M. B., González, A. G. A., Iváncsy, T. "The effects of the corona wire distribution with triangular collecting plates on the characteristics of electrostatic precipitators", In: 2022 International Conference on Diagnostics in Electrical Engineering (Diagnostika), Pilsen, Czech Republic, 2022, pp. 1–7. ISBN 978-1-6654-8083-3
https://doi.org/10.1109/Diagnostika55131.2022.9905103

[16] González, A. G. A., Fayyad, M. B., Iváncsy, T. "The effect of corona wire position and radius in a duct-type ESP with wavy collecting plates", International Journal of Electrical and Electronic Engineering & Telecommunications (IJEETC), 11(4), pp. 262–268, 2022.
https://doi.org/10.18178/ijeetc.11.4.262-268

[17] COMSOL Multiphysics 6.1 "Electrostatic Precipitator", [pdf] COMSOL, Inc., 2022. Available at: https://www.comsol.com/model/download/1087061/models.plasma.electrostatic_precipitator.pdf [Accessed: 27 January 2023]

[18] Potrymai, E., Perstnov, I. "Time Dependent Modelling and Simulation of the Corona Discharge in Electrostatic Precipitators", MSc Thesis, Linnaeus University, 2014.

[19] Rubinetti, D., Weiss, D., Egli, W. "Corona discharge - A fully coupled numerical approach verified and validated", The International Journal of Multiphysics, 11(4), pp. 375–386, 2017.
https://doi.org/10.21152/1750-9548.11.4.375

[20] Lawless, P. A. "Particle charging bounds, symmetry relations, and an analytic charging rate model for the continuum regime", Journal of Aerosol Science, 27(2), pp. 191–215, 1996.
https://doi.org/10.1016/0021-8502(95)00541-2

[21] Zheng, C., Zhang, X., Yang, Z., Liang, C., Guo, Y., Wang, Y., Gao, X. "Numerical simulation of corona discharge and particle transport behavior with the particle space charge effect", Journal of Aerosol Science, 118, pp. 22–33, 2018.
https://doi.org/10.1016/j.jaerosci.2018.01.008

[22] Dong, M., Zhou, F., Zhang, Y., Shang, Y., Li, S. "Numerical study on fine-particle charging and transport behaviour in electrostatic precipitators", Powder Technology, 330, pp. 210–218, 2018.
https://doi.org/10.1016/j.powtec.2018.02.038

[23] Li, S., Huang, Y., Zheng, Q., Deng, G., Yan, K. "A numerical model for predicting particle collection efficiency of electrostatic precipitators", Powder Technology, 347, pp. 170–178, 2019.
https://doi.org/10.1016/j.powtec.2019.02.040

[24] Świerczok, A., Jędrusik, M. "The collection efficiency of ESP model - Comparison of experimental results and calculations using Deutsch model", Journal of Electrostatics, 91, pp. 41–47, 2018.
https://doi.org/10.1016/j.elstat.2017.12.004

[25] He, Z., Dass, E. T. M. "Correlation of design parameters with performance for electrostatic Precipitator. Part I. 3D model development and validation", Applied Mathematical Modelling, 57, pp. 633–655, 2018.
https://doi.org/10.1016/j.apm.2017.05.042